5.2 Wavefront coherence time

5.2.1 Validation sample

All the scattered plots for the wavefront coherence time τ_0 are summarized in Figure 54 (read the caption for more details). We had two different instruments (MASS and DIMM) that run simultaneously on a number of nights of the validation sample. Tables 88 and 89 report the contingency tables between MASS and DIMM for τ_0 (48 nights in 2010/2011). In the first table the DIMM is taken as a reference, in the second table the MASS is taken as a reference. Tables 90 is the contingency table between Meso-NH and DIMM for the 42 nights (over the total of 89 nights of the validation sample) related to summer. Tables 91 is the contingency table between Meso-NH and DIMM for the 47 nights (over the total of 89 nights of the validation sample) related to winter. Tables 92 is the contingency table between Meso-NH and MASS for the 21 nights (over the total of 48 nights of the validation sample) related to summer. Tables 93 is the contingency table between Meso-NH and MASS for the 27 nights (over the total of 48 nights of the validation sample) related to winter. Table 92 and Table 93 have been calculated using the data corrected as in Fig.54-(f) and (g). There are no MASS data available for 2007, therefore we could not analyse τ_0 for this sub-sample.

If we look at POD_3 that is the probability to forecast the wavefront coherence time that is larger than the third tertile (the most interesting case from an astronomical point of view because this corresponds to the cases in which an AO system can be run at lower temporal frequency) we can observe that we obtain, in all cases, very good results. POD_3 is 70.73 % for Meso-Nh-DIMM (summer time, Table 90) and 65.63 % for Meso-Nh-DIMM (winter time, Table 91). POD_3 is 71.87 % for Meso-Nh-MASS (summer time, Table 92) and 78.20 % for Meso-Nh-MASS (winter time, Table 93). Also the values of POD_1 that tell us the probability to detect a τ_0 weaker than the first tertile is very satisfactory included in the range [48-69] % depending of the instrument we take as a reference.

For what concerns the scattering plots, we note that the values of σ obtained between DIMM and MASS and the Meso-Nh with MASS and Meso-Nh with DIMM are comparable. In some cases the σ of Meso-Nh with the instrument (Meso-Nh with DIMM in summer and winter: σ respectively 1.66 ms and 1.20 ms) is even smaller than that obtained considering the two instrument (σ=1.73 ms).

It is important to highlight that, as it can be seen in Fig.54-(a) there is a residual bias between the DIMM and MASS measurements. This indicates that there are uncertainties in measurements that we can not neglect highly probably due to the fact that in one or two techniques there are still some things to arrange. We do not enter in details of this issue here (a few indications can be found in [54] for the MASS) because this is not the main goal of this report. The important thing is that, once one assumes that the reference is one or the other instrument, the model predicts the values with a good score of success.

	τ_0 48 nights	**DIMM** $\tau_0 < 2.07ms$	$2.07ms < \tau_0 < 3.26ms$	$\tau_0 > 3.26ms$
MASS	$\tau_0 < 2.07ms$	182	15	8
	$2.07ms < \tau_0 < 3.26ms$	167	139	16
	$\tau_0 > 3.26ms$	46	240	370

Total points = 1183; PC=58.41%; EBD=4.56%
POD_1=46.08%; POD_2=35.28%; POD_3=93.91%

Table 88: Contingency table of τ_0 between MASS and DIMM, using the DIMM as a reference (48 nights in 2010/2011) - validation sample.

	τ_0 48 nights	**MASS** $\tau_0 < 2.68ms$	$2.68ms < \tau_0 < 4.87ms$	$\tau_0 > 4.87ms$
DIMM	$\tau_0 < 2.68ms$	364	215	65
	$2.68ms < \tau_0 < 4.87ms$	20	170	226
	$\tau_0 > 4.87ms$	11	9	103

Total points = 1183; PC=53.85%; EBD=6.42%
POD_1=92.15%; POD_2=43.15%; POD_3=26.14%

Table 89: Contingency table of τ_0 between MASS and DIMM, using the MASS as a reference (48 nights in 2010/2011) - validation sample.

	$\tau_0 - SUMMER$ 42 nights over 89	**DIMM** $\tau_0 < 2.20ms$	$2.20ms < \tau_0 < 3.58ms$	$\tau_0 > 3.58ms$
MNH	$\tau_0 < 2.20ms$	178	61	13
	$2.20ms < \tau_0 < 3.58ms$	138	139	95
	$\tau_0 > 3.58ms$	54	169	261

Total points = 1108; PC=57.17%; EBD=6.05%
POD_1=48.11%; POD_2=37.67%; POD_3=70.73%

Table 90: Contingency table of τ_0 between Meso-NH and DIMM, in summer - validation sample.

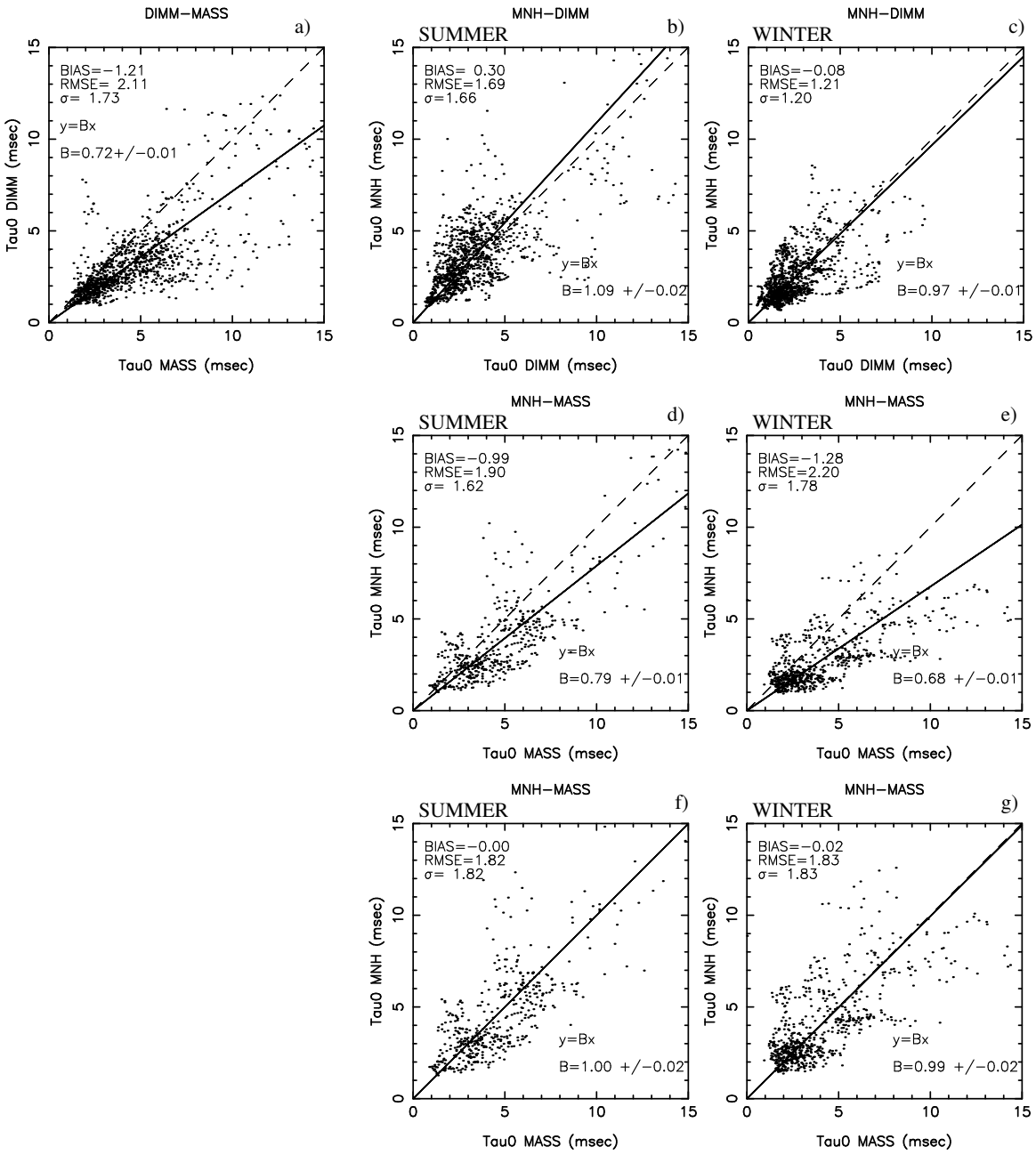

Figure 54: Scattered plots (validation sample) of the wavefront coherence time for (a) 48 nights in 2010/1011 (there are no MASS measurements in 2007) between MASS and DIMM; (b) 42 nights in 2010/2011 between Meso-NH and DIMM in summer; (c) 47 nights in 2010/2011 between Meso-NH and DIMM in winter; (d) 21 nights in 2010/2011 between Meso-NH and MASS in summer; (e) 27 nights in 2010/2011 between Meso-NH and MASS in winter; (f) the same as (d) but with the MASS corrected using the coefficient of the regression line from (d); and (g) the same as (e) but with the MASS corrected using the coefficient of the regression line from (e).

	$\tau_0 - WINTER$ 47 nights over 89	**DIMM** $\tau_0 < 1.67ms$	$1.67ms < \tau_0 < 2.48ms$	$\tau_0 > 2.48ms$
MNH	$\tau_0 < 1.67ms$	271	187	37
	$1.67ms < \tau_0 < 2.48ms$	118	116	107
	$\tau_0 > 2.48ms$	31	116	275

Total points = 1258; PC=52.62%; EBD=5.40%
POD_1=64.52%; POD_2=27.68%; POD_3=65.63%

Table 91: Contingency table of τ_0 between Meso-NH and DIMM, in winter - validation sample.

	$\tau_0 - SUMMER$ 21 nights over 48	**MASS** $\tau_0 < 3.27ms$	$3.27ms < \tau_0 < 5.36ms$	$\tau_0 > 5.36ms$
MNH	$\tau_0 < 3.27ms$	111	70	7
	$3.27ms < \tau_0 < 5.36ms$	49	52	38
	$\tau_0 > 5.36ms$	1	38	115

Total points = 481; PC=57.80%; EBD=1.66%
POD_1=68.94%; POD_2=32.50%; POD_3=71.87%

Table 92: Contingency table of τ_0 between Meso-NH and MASS, in summer - validation sample.

	$\tau_0 - WINTER$ 27 nights over 48	**MASS** $\tau_0 < 2.45ms$	$2.45ms < \tau_0 < 4.19ms$	$\tau_0 > 4.19ms$
MNH	$\tau_0 < 2.45ms$	112	86	6
	$2.45ms < \tau_0 < 4.19ms$	94	108	45
	$\tau_0 > 4.19ms$	28	40	183

Total points = 702; PC=57.41%; EBD=4.84%
POD_1=47.86%; POD_2=46.15%; POD_3=78.20%

Table 93: Contingency table of τ_0 between Meso-NH and MASS, in winter - validation sample.

5.2.2 Calibration sample

Tables 94, 95, 96, 97, 98, and 99 report the contingency tables of τ_0 for all the comparisons between the instruments (MASS, DIMM and GS) for the calibration sample.

	τ_0 14 nights	**MASS** $\tau_0 < 2.30ms$	$2.30ms < \tau_0 < 5.14ms$	$\tau_0 > 5.14ms$
DIMM	$\tau_0 < 2.30ms$	89	28	0
	$2.30ms < \tau_0 < 5.14ms$	0	57	79
	$\tau 0 > 5.14ms$	0	4	9

Total points = 266; PC=58.27%; EBD=0%
POD_1=100%; POD_2=64.04%; POD_3=10.23%

Table 94: Contingency table of τ_0 between MASS and DIMM (14 nights of the calibration sample in 2007), using the MASS as a reference.

	τ_0 14 nights	**DIMM** $\tau_0 < 1.63ms$	$1.63ms < \tau_0 < 3.35ms$	$\tau_0 > 3.35ms$
MASS	$\tau_0 < 1.63ms$	47	0	0
	$1.63ms < \tau_0 < 3.35ms$	42	42	1
	$\tau_0 > 3.35ms$	0	47	87

Total points = 266; PC=66.16%; EBD=0%
POD_1=52.81%; POD_2=47.19%; POD_3=98.86%

Table 95: Contingency table of τ_0 between MASS and DIMM (14 nights of the calibration sample in 2007), using the DIMM as a reference.

A detailed analysis of the contingency tables calculated on the calibration sample does not provide interesting new results with respect to what we have already observed on the validation sample that in any case remains the most representative sample. The only useful thing that deserves to be highlighted is that, in calibration sample, we had three different instruments (the DIMM, the MASS and the GS) running simultaneously. We could therefore calculate different combinations with permutation for the contingency tables. On the other side, looking at both scattering plots (Fig.55) and contingency tables of each couple: MASS-DIMM, DIMM-GS, GS-MASS (Table 94-Table 99), it is possible to observe that the calculation of τ_0 by the DIMM and the MASS have to be treated with precaution. The MASS seems well correlated to the GS (differently from the DIMM). However this is only a limited sample of just 14 nights. In a detailed analysis of the inter-comparison between MASS and GS [54] we proved that the MASS shows tendency in overestimating the τ_0 for large τ_0 (> 5 ms). We therefore just recommend precaution in treating τ_0 retrieved from DIMM and MASS. **We simply note that the contingency table of the model Meso-Nh with the GS (Table 100) that is most realiable instrument for τ_0 provides very satisfactory results with all the POD$_i$ in the range [56.55, 88.09] %. This result, joint with the even more useful results obtained with the validation sample described in 5.2.1, indicate that the τ_0 is at present well reconstructed by the model in summer as well as in winter time**.

	τ_0 20 nights	GS $\tau_0 < 2.86ms$	GS $2.86ms < \tau_0 < 4.74ms$	GS $\tau_0 > 4.74ms$
DIMM	$\tau_0 < 2.86ms$	166	123	28
	$2.86ms < \tau_0 < 4.74ms$	2	41	111
	$\tau_0 > 4.74ms$	0	4	29

Total points = 504; PC=46.82%; EBD=5.55%
POD_1=98.81%; POD_2=24.40%; POD_3=17.26%

Table 96: Contingency table of τ_0 between GS and DIMM (20 nights of the calibration sample in 2007), using the GS as a reference.

	τ_0 20 nights	DIMM $\tau_0 < 1.63ms$	DIMM $1.63ms < \tau_0 < 3.07ms$	DIMM $\tau_0 > 3.07ms$
GS	$\tau 0 < 1.63ms$	55	3	1
	$1.63ms < \tau_0 < 3.07ms$	86	43	4
	$\tau_0 > 3.07ms$	27	122	163

Total points = 504; PC=51.79%; EBD=5.55%
POD_1=32.74%; POD_2=25.60%; POD_3=97.02%

Table 97: Contingency table of τ_0 between GS and DIMM (20 nights of the calibration sample in 2007), using the DIMM as a reference.

	τ_0 14 nights	GS $\tau_0 < 2.96ms$	GS $2.96ms < \tau_0 < 5.44ms$	GS $\tau_0 > 5.44ms$
MASS	$\tau_0 < 2.96ms$	78	39	0
	$2.96ms < \tau_0 < 5.44ms$	8	37	20
	$\tau_0 > 5.44ms$	0	10	66

Total points = 258; PC=70.15%; EBD=0%
POD_1=90.70%; POD_2=43.02%; POD_3=76.74%

Table 98: Contingency table of τ_0 between GS and MASS (14 nights of the calibration sample in 2007), using the GS as a reference.

	τ_0 14 nights	MASS $\tau_0 < 2.31ms$	MASS $2.31ms < \tau_0 < 5.21ms$	MASS $\tau_0 > 5.21ms$
GS	$\tau_0 < 2.31ms$	50	10	0
GS	$2.31ms < \tau_0 < 5.21ms$	36	63	10
GS	$\tau_0 > 5.21ms$	0	13	6

Total points = 258; PC=73.26%; EBD=0%
POD_1=58.14%; POD_2=73.26%; POD_3=88.37%

Table 99: Contingency table of τ_0 between GS and MASS (14 nights of the calibration sample in 2007), using the MASS as a reference.

	τ_0 20 nights	GS $\tau_0 < 2.86ms$	GS $2.86ms < \tau_0 < 4.73ms$	GS $\tau_0 > 4.73ms$
MODEL	$\tau_0 < 2.86ms$	148	47	1
MODEL	$2.86ms < \tau_0 < 4.73ms$	20	95	58
MODEL	$\tau_0 > 4.73ms$	0	26	109

Total points = 504; PC=69.84%; EBD=0.19%
POD_1=88.09%; POD_2=56.55%; POD_3=64.88%

Table 100: Contingency table of τ_0 between GS and Meso-NH (20 nights of the calibration sample in 2007).

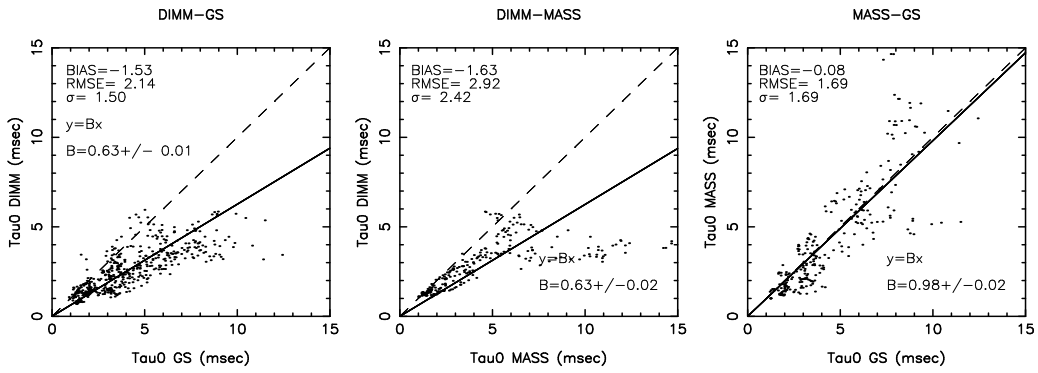

Figure 55: Scattered plot of the τ_0 between DIMM and GS (left), DIMM and MASS (centre) and GS and MASS (right) for the calibration sample of 20 nights.

5.3 Isoplanatic angle

5.3.1 Validation sample

The isoplanatic angle, as the seeing, resulted sensitive to the seasonal model calibration. We present therefore here, as we did for the seeing, the results obtained for the summer. In Figure 56 are reported the scattered plots of θ_0 between DIMM and MASS on a sample of 44 nights in 2010/2011 (figure on left) and between MASS and Meso-NH for the summer sample corresponding to 21 nights over the total sample of 48 nights in 2010/2011 (figure on the right). Table 101 and 102 are the contingency tables for θ_0 between MASS and DIMM for the 44 nights in 2010/2011. Table 103 is the contingency table between Meso-NH and MASS, during summer (21 nights over 48 nights), for θ_0. Observing the scattering plots of Fig.56 we note that the two figures have a comparable value for σ (0.48" vs. 0.56") even if measurements are better correlated among them than what is observed between the Meso-Nh model and the MASS. The cloud of points in the picture on the left is indeed better elongated along the regression line. On the other side it is possible to observe that the model has visibly improved its performances for the reconstruction of θ_0 and the serious problem of the 'flat' distribution of the cloud of points that we had obtained at the end of Phase A (before the modification of the algorithm of the calculation of the C_N^2) has been overcome. The model arrives to reconstruct a vertical stratification of the turbulence in the free atmosphere with a much higher temporal variability with a θ_0 spread on the same interval of measurements (typically [1,3] arcsec)[1] as noted in the scattering plot. Even if there is still space for improvements, the results is now definitely satisfactory providing comparable σ values with measurements. As for the τ_0 we observe that the MASS and DIMM distribution of points presents a not negligible bias. However, for the θ_0 the recent study from Masciadri et al., 2014 ([54]) indicates that the MASS seems to be better reliable than the DIMM. We calculated therefore the contingency table between the Meso-Nh and the MASS (Table 103). **We observe that the percentage of the $\mathbf{POD}_i$ is definitely improved with the new C_N^2 algorithm. Before the modification of the algorithm we had $\mathbf{POD}_1$ and $\mathbf{POD}_3$ basically equal to zero because the distribution of the points in the scattering plot was very flat. After the modification of the algorithm of the C_N^2, the model performances improved in a drastic way (see Table 103). Also we remind that, from an astronomical point of view, it is particularly interesting to be able to identify temporal windows with large θ_0 because those intervals are favorable for observations supported by GLAO, MCAO and WFAO. The most interesting parameter is therefore $\mathbf{POD}_3$ that is the probability that the model detect a θ_0 larger than the third tertile. Our estimate of $\mathbf{POD}_3$ is pretty satisfactory because is of the order of 58.80** %. POD_1 is still weak and this tells us that there is still space for improvements (even if POD_1 is definitely less critical from the 'flexible-scheduling' point of view). A collaboration with our colleagues of CNRM-Toulouse is on-going on this subject and we are confident we will be able to improve the model performances in the future.

In order to appreciate the improvement of the model in reconstructing the temporal evolution of the turbulence in the free atmosphere we report in Fig.57 the temporal evolution of the θ_0 in a few nights of the sample of 48 nights (2010/2011). These are raw model outputs, before to apply the moving average of 1 hour and the temporal resampling of 20 minutes. If we compare with Fig.41 (left) of MOSE Report Phase A, the improvement of model performances is definitely evident.

5.3.2 Calibration sample

As for the τ_0 the analysis of the contingency tables and scattering plots for θ_0 does not provide any useful and interesting results. The validation sample is statistically richer than the calibration sample. Even more important the the validation sample is independent from the calibration sample. On the other side we found interesting the analysis of the temporal evolution of the θ_0 simulated by the model and measured by GS, DIMM and MASS on the 20 nights of the calibration sample. In Fig.58 and Fig.59 we can see that the red line (model) is not flat anymore but it evolves in a much better agreement with measurements.

[1] We remind to the reader that measurements and simulations are treated with a moving average of 1 hour plus a resampling of 20 minutes

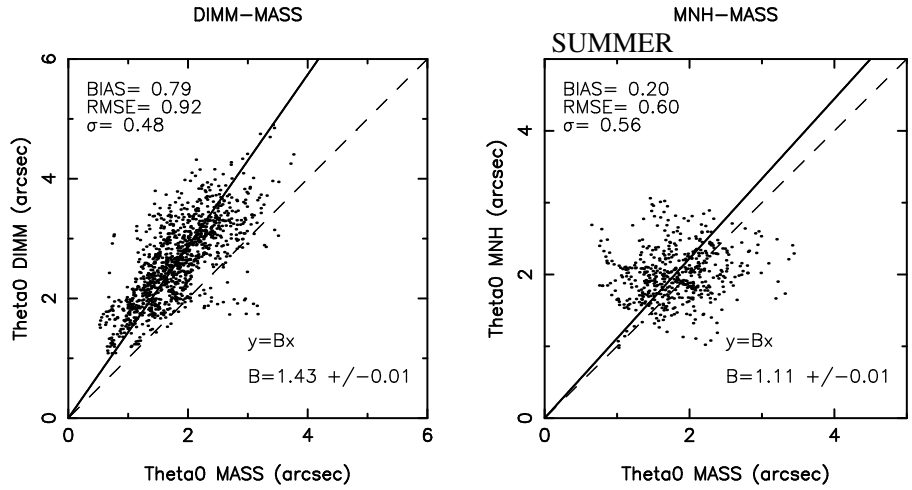

Figure 56: Scattered plots of the isoplanatic angle θ_0 between DIMM and MASS (left figure) and between MASS and Meso-NH (on the right, for the summer sample only).

	θ_0	**MASS**		
	44 nights	$\theta_0 < 1.53$"	1.53" $< \theta_0 <$ 2.04"	$\theta_0 > 2.04$"
DIMM	$\theta_0 < 1.53$"	47	1	0
	1.53" $< \theta_0 <$ 2.04"	157	45	17
	$\theta_0 > 2.04$"	168	325	354

Total points = 1114; PC=40.04%; EBD=15.08%
POD_1=12.63%; POD_2=12.13%; POD_3=95.42%

Table 101: Contingency table of θ_0 between MASS and DIMM, using the MASS as a reference (44 nights in 2010/2011).

5.4 Conclusions

The conclusion of our analysis on the performances of the new algorithm of the C_N^2 implemented in the Meso-Nh model can be summarized as it follows.

- The **wavefront coherence time (τ_0)** is the parameter that at present is predicted with the best score of success. All the POD$_i$ (i = 1, 2 and 3) are satisfactory and comparable to those obtained among different instruments, in some cases even better. From a scientific point of view, for τ_0 the most interesting POD is POD$_3$ that is the probability to detect a τ_0 larger than the third tertile. **POD$_3$ on the validation sample is included in the range [72% - 78%] if we considered the most reliable instrument as a reference i.e. the MASS**. The range includes the analysis done in different seasons: summer and winter. The samples we are dealing about include 42 nights (summer) and 47 nights (winter). POD$_1$ is included in the range [48% - 69%] using as a reference the same instrument. Another not negligible favorable point for τ_0 is that this score of success has been obtained with just one model calibration (i.e. not a calibration for summer and one for winter) and we analyzed data in summer as well as in winter. It will be interesting to evaluate if this score of success will further improve with a seasonal calibration.

  The ability to detect a large τ_0 in advance is extremely useful for the following reasons. A large τ_0 permits

	θ_0 44 nights	DIMM $\theta_0 < 2.26$"	DIMM 2.26" $< \theta_0 <$ 2.94"	DIMM $\theta_0 > 2.94$"
MASS	$\theta_0 < 2.26$"	354	329	177
MASS	2.26" $< \theta_0 <$ 2.94"	13	38	156
MASS	$\theta_0 > 2.94$"	5	4	38

Total points = 1114; PC=38.60%; EBD=16.34%
POD_1=95.16%; POD_2=10.24%; POD_3=10.24%

Table 102: Contingency table of θ_0 between MASS and DIMM, using the DIMM as a reference (44 nights in 2010/2011).

	$\theta_0 - SUMMER$ 21 nights over 48	MASS $\theta_0 < 1.55$"	MASS 1.55" $< \theta_0 <$ 2.01"	MASS $\theta_0 > 2.01$"
MNH	$\theta_0 < 1.55$"	16	18	12
MNH	1.55" $< \theta_0 <$ 2.05"	88	80	61
MNH	$\theta_0 > 2.05$"	70	75	100

Total points = 520; PC=37.69%; EBD=15.77%
POD_1=9.20%; POD_2=46.24%; POD_3=57.80%

Table 103: Contingency table of θ_0 between MASS and Meso-NH (21 summer nights in 2010/2011)

an AO system to run at lower temporal frequency and to use fainter stars as a guide stars. A lower temporal frequency permits indeed to better sample light coming from stars that with a smaller τ_0 can not simply be used as guide stars. This represents an advantage for the wide field AO because the number of available guide stars increases and because a higher SR is reachable (see Annex B) and more ambitious scientific project can be carried out. It is also an advantage for classical SCAO configuration because it permits to observe fainter stars reaching a higher SR.

- The **total seeing (ε)** revealed to be sensitive to the seasonal model calibration. This means that the model needs a twofold calibration: one for summer and one for winter. We provided therefore in this study only the score of success for the summer time because the calibration sample belongs to this season. We will be able to use the measurements of the site testing campaign planned for Paranal with a Stereo-SCIDAR to calibrate the model for the winter time. In the case of the seeing, the most interesting POD from a scientific point of view is POD_1. **The probability to detect the $\varepsilon <$ 1" is in the range [62% - 72%]. The probability to detect the $\varepsilon <$ of the first tertile is in the range [48% - 53%]**. The range in this case has the following meaning: the most conservative values (62% and 48% have been obtained with the sample of 42 nights (summer) in the 2010/2011 years. The most optimistic values have been obtained with the sub-sample of the 18 nights (summer) of 2007 (the same year in which the calibration sample belongs). The instrument used as a reference was the DIMM.

  The advantage in detecting in advance a weak ε is obvious. The best seeing conditions guarantee the highest SR of an AO system and the most challenging scientific programs such as the search and the characterization of extrasolar planets would definitely gain from this condition.

- The **isoplanatic angle (θ_0)**, as the seeing, revealed to be sensitive to the seasonal model calibration. We provide therefore in this study only the score of success for the summer for the same reason described

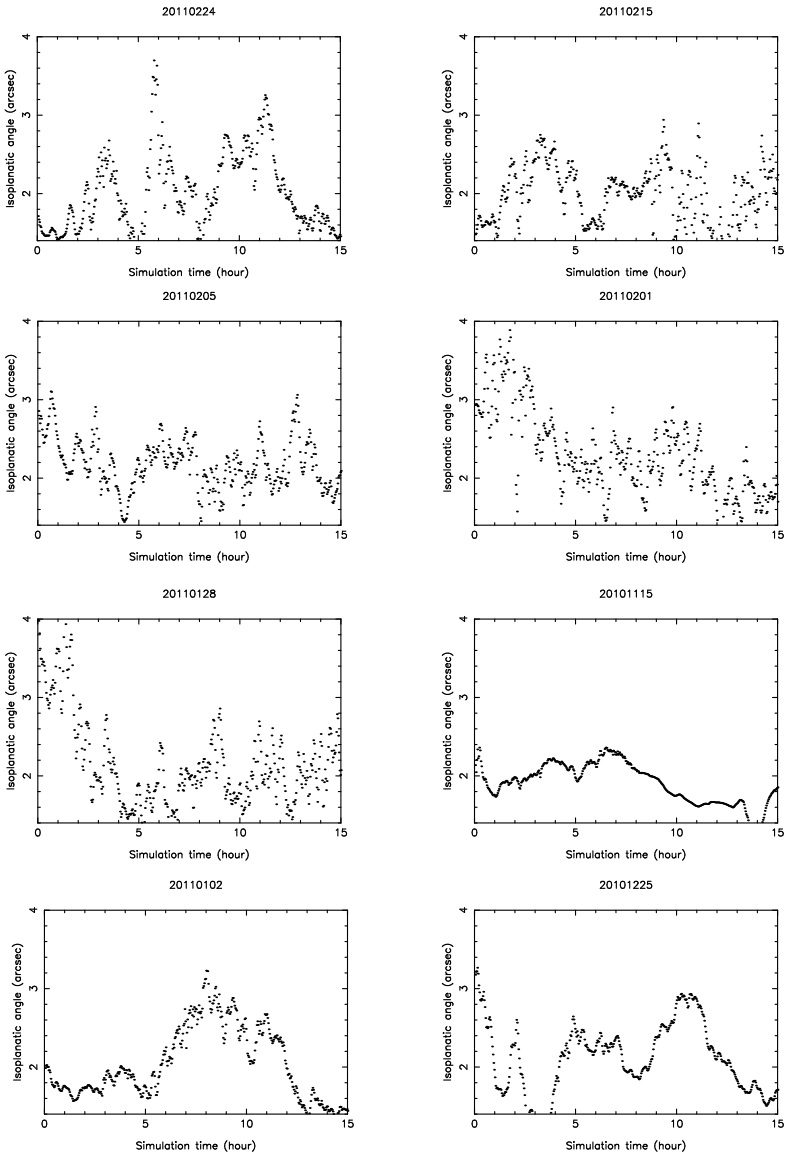

Figure 57: Temporal evolution of the isoplanatic angle (θ_0) in a few nights of the validation sample (48 nights in summer time).

for the seeing. From a scientific point of view, for θ_0 the most interesting POD is POD_3 that is the probability to detect a θ_0 larger than the third tertile. **POD_3 on the validation sample is equal to 58% if we considered as a reference the MASS**. The samples we are dealing about include 21 nights (summer) of (2010/2011). No measurements with MASS are available for 2007. For completeness we also note that, at present, the probability to detect an isoplanatic angle smaller than the first tertile (POD_1) is not sufficiently good ($\sim 9\%$). This seems to come from the fact that the first tertile of Meso-Nh is slightly larger than that of measurements. We plan to undertake further investigations to improve this score of success. At the same time we highlight the fact that, from a scientific point of view, POD_3 is definitely more interesting than POD_1.

A large value of the θ_0 is particularly useful for whatever kind of wide field AO (GLAO, MCAO, etc...). Observations supported by AO systems of extended and crowded fields such as clusters would definitely

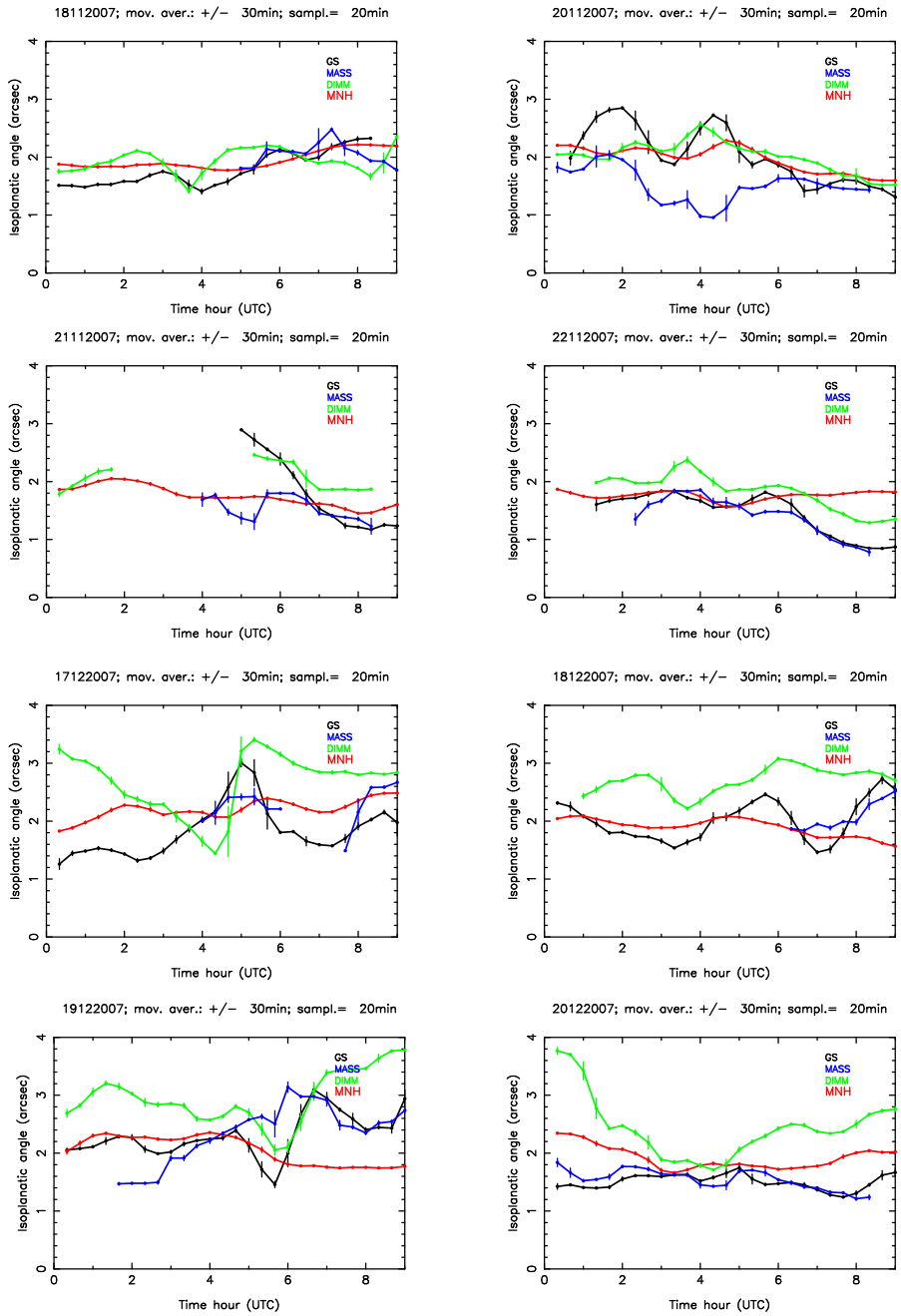

Figure 58: Temporal evolution of the isoplanatic angle (θ_0) in all the nights of the calibration sample (20 nights). Red: Meso-h model, Black: Generalized SCIDAR, Green: DIMM, Blue: MASS. All measurements and simulations are treated with a moving average of 1 hour plus a resampling of 20 minutes.

benefit from this condition if it would be known in advance.

- It is important to note that the new algorithm proposed for the C_N^2 it is basically built in a way to preserve the good performances obtained with the model using the standard algorithm (for example the prediction of the seeing and the wavefront coherence time) and to improve its performances in those contexts where it showed some weak performances (typically a low temporal variability of the turbulence

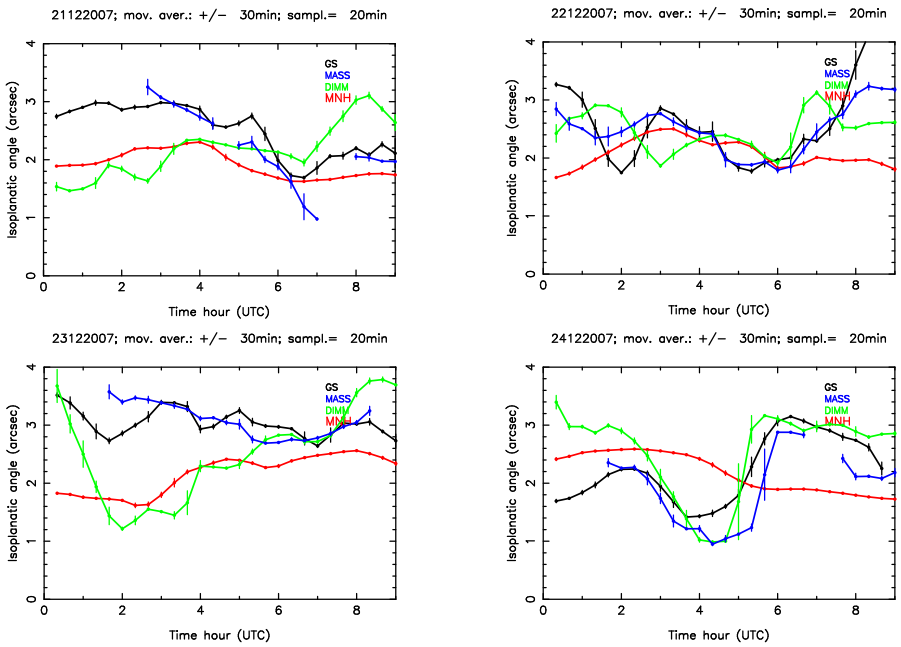

Figure 59: As for Fig.58.

in the free atmosphere). Since the seeing is mainly driven by the turbulence close to the ground (h < 700 m), the good seeing prediction is preserved with the new algorithm because it changes only for h > 700 m. This means that the seeing remains almost the same with the standard and the new algorithm. The differences are definitely negligible. We report the values of the most significative POD_1 for the seeing in **summer time**: POD_1= 62.03% with the standard algorithm, POD_1= 63.97% with the new algorithm. More difficult is to predict how the τ_0 changes because it depends on both factors (C_N^2 and wind speed). For this reason we had to calculate the contingency tables in both cases. We report here only the POD_3

(for sake of readability) for the case we use the standard and the new algorithm and we observed that it is substantially preserved and it is even better with the new algorithm. POD_3 is the most significative POD for the τ_0. In **summer time**, if we consider MNH vs. DIMM the POD_3=68.83% with the standard algorithm and 70.73% with the new algorithm. In summer time, if we consider MNH vs. MASS the POD_3=61.87% with the standard algorithm and 71.87% with the new algorithm. In **winter time**, if we consider MNH vs. DIMM the POD_3=60.61% with the standard algorithm and 65.63% with the new algorithm. In winter time, if we consider MNH vs. MASS the POD_3=59.40% with the standard algorithm and 78.20% with the new algorithm.

5.5 The fraction of turbulence energy in the first 600 m

In this section we report, in form of a snapshot a couple of considerations. This is not part of the deliverables of the project but it is certainly an interesting element in the framework of the applications to the Service Mode of facilities assisted by AO systems. In Fig.60-right is reported, for a sample of a few nights of the site testing campaign PAR2007, the temporal evolution of the fraction of turbulence energy in the first 600 m defined as J_{600}/J_{TOT} as reconstructed by the Meso-Nh model and as observed by the Generalized SCIDAR. In Fig.60-left is reported the temporal evolution of the total seeing as observed by the DIMM and the GS and reconstructed by the model. These are all cases in which the model can visibly reconstruct in a pretty good way the fraction of energy in the first 600 m above the ground. This quantity is particularly useful in application to WFAO systems and in particular to the AOF.

We did not use the MASS-DIMM as a reference because, as discussed/proved in Masciadri et al., 2014 [54], the subtraction of the MASS from the DIMM can hardly provide an accurate estimate of the turbulence below a precise pre-defined height. This is mainly because **(1)** the MASS shows a tendency in underestimating the turbulence in the free atmosphere and **(2)** because it is not possible to define a precise height above the ground that can divide the atmosphere in two vertical slabs. This is due to an intrinsic limitation related to the principle on which the method of measurement is based on. The MASS-DIMM measurements are therefore not a good reference. On the other side, this is the unique monitor existent at present and the unique monitor that ESO is using for this kind of estimations. We can not exclude there will be a method to fit the J of the free atmosphere retrieved from the MASS-DIMM with the GS ones. However this should be an artificial solution (from a conceptual point of view) based on the assumption that one corrects/modifies the MASS data taking as a reference the GS. Even more critical is the identification of a precise height as a threshold that discriminates the low and high part of the atmosphere.

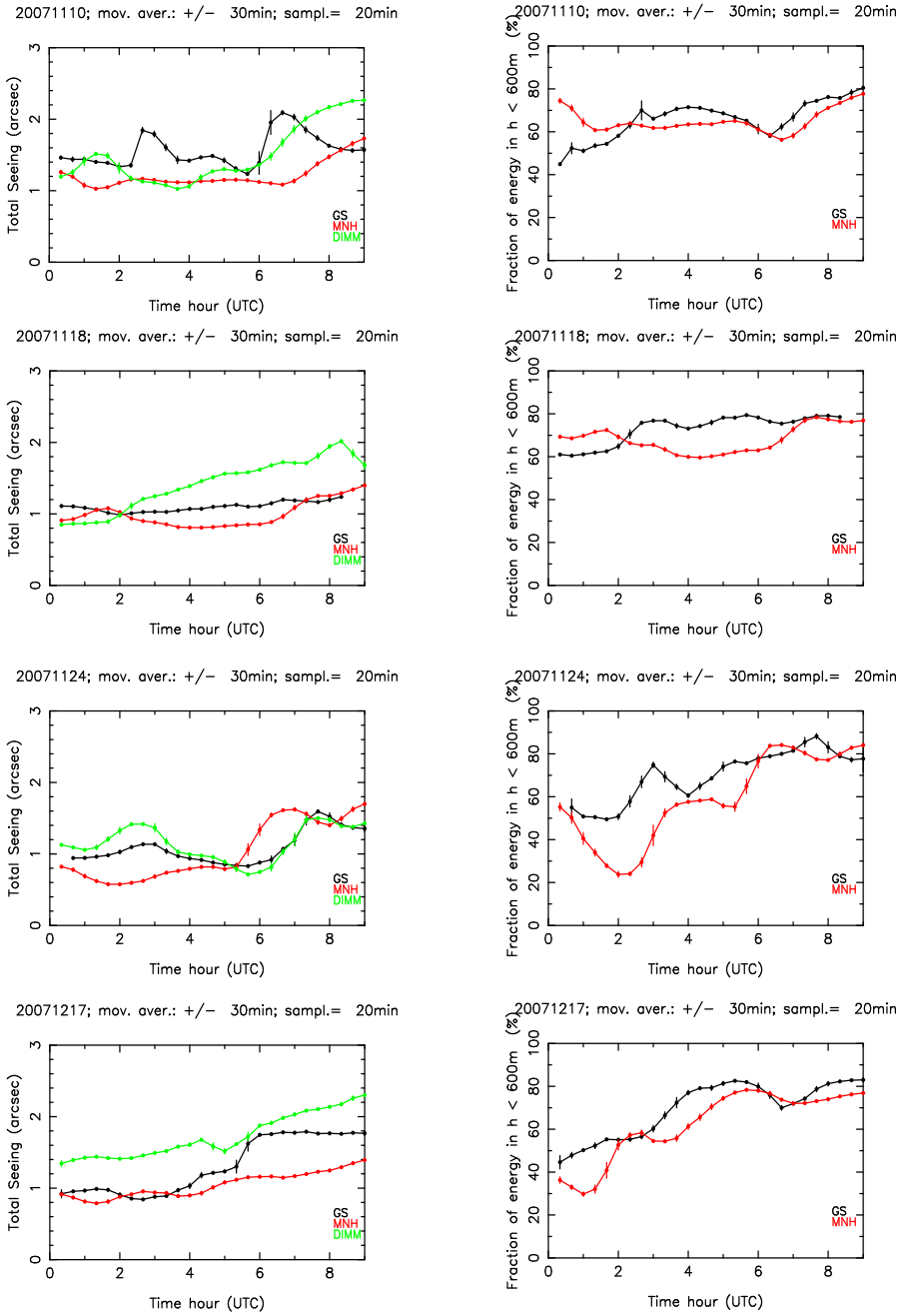

Figure 60: Left: temporal evolution of the total seeing as observed by DIMM (green line) and the Generalized SCIDAR (black line) and reconstructed by the Astro-Meso-nh model (red line). Right: temporal evolution of the fraction of the turbulence energy in the first 600 m as observed by the Generalized-SCIDAR (black line)and reconstructed by the model (red line).

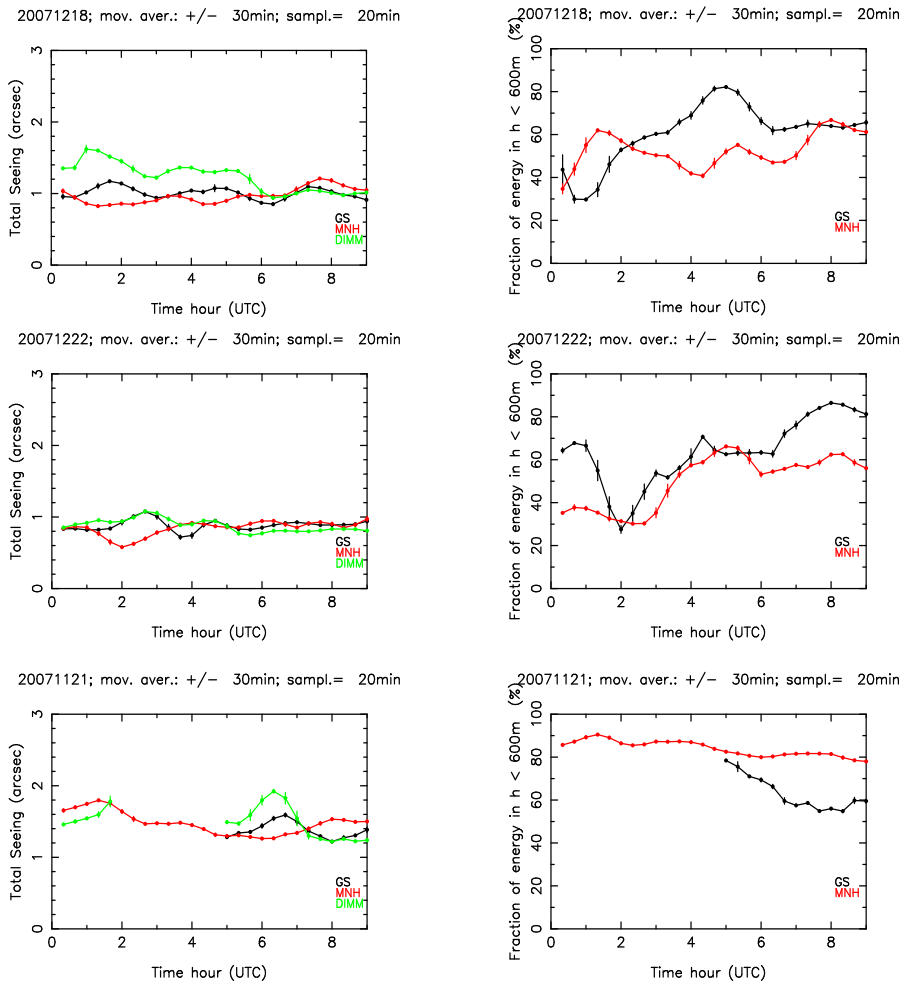

Figure 61: As for Fig.60.

6 Work Package 2.2 - 137 vertical levels in initialization data

Studies done so far covering years from 2007 to 2011 used, as initialization and forcing data, ECMWF analyses and forecasts having 91 vertical levels. Such an intrinsic vertical resolution permits to achieve a maximum vertical resolution in the free atmosphere of the order of $\sim$ 300 m. Knowing that 62 levels (the resolution used at present with Meso-NH) corresponds in the free atmosphere more or less to 600 m one can hope to improve the vertical resolution of the C_N^2 using a larger number of vertical levels with Meso-Nh. Of course a number of levels much larger than those necessary to resolve 300 m should not produce a better vertical resolution or to resolve thinner C_N^2 layers. This concept is well visible in Fig.62 where are shown three different C_N^2 profiles (obtained by the way with the standard C_N^2 algorithm) in which the vertical resolution of Meso-Nh is 62, 99 and 173 levels. We observe differences in the vertical C_N^2 stratification passing from 62 to 99 levels because the intrinsic resolution of the ECMWF data have a higher resolution than that of 62 levels of Meso-Nh in the center of the free atmosphere. There is therefore space to detect further thermodynamical instabilities if we pass from 62 to 99 levels. We do not observe substantial changes in the stratification passing from 99 to 173 levels because the intrinsic resolution is given by the 91 vertical levels of the ECMWF products and is we pass from 99 to 173 levels we are simply oversampling the vertical profile[2].

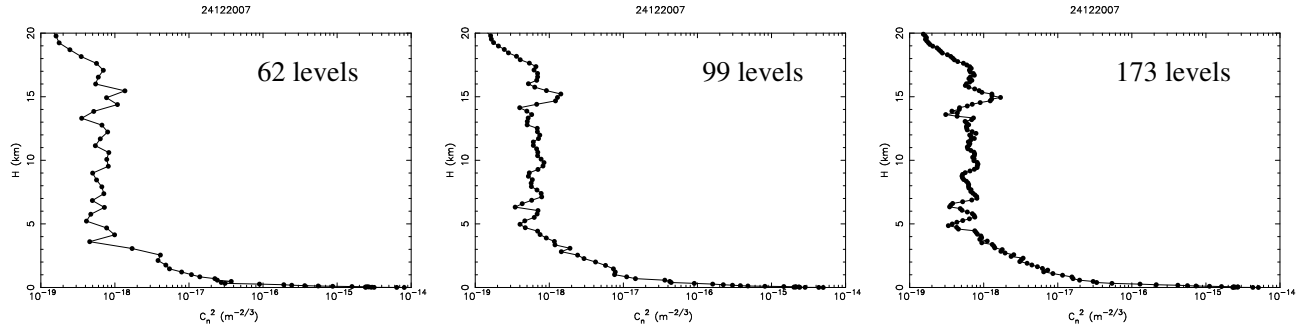

Figure 62: Vertical profiles of the average simulated C_N^2 with different vertical resolutions, for a night in 2007. Left: with 62 levels; Middle: with 99 levels; Right: with 173 levels.

The investigation of the sensitivity of the C_N^2 as a function of the vertical resolution had originally be planned in Phase B to verify if a higher vertical resolution could improve the temporal variability of the turbulence in the free atmosphere. As we will see in this section, after the modification of the C_N^2 algorithm we observed that also with 62 vertical levels of Meso-Nh the temporal variability of the seeing in the free atmosphere is sufficiently good. **However, if we use a larger number of vertical levels we are able to resolve turbulent layers as thin as 150 m in the free atmosphere with a a good temporal variability. This achievement is particularly interesting for the applications to the WFAO (AOF) and certainly opens new perspectives for the future**.
Since 25/6/2013, ECMWF analyses and forecasts have 137 vertical levels. Such a vertical stratification should permit to increase the vertical resolution of Meso-Nh up to $\sim$ 150 m provided the number of the Meso-Nh vertical levels increases opportunely. To investigate which kind of impact would have produced a simulation done with Meso-Nh using a larger number of vertical levels we selected two nights (more recent than 25/6/2013) and we performed a double simulation with Meso-Nh with 62 and 173 levels for each night. Figures 63 shows the C_N^2 vertical profiles extended on the whole atmosphere 0-20km (left) and in the first kilometer above the ground (right) in two nights: 15/12/2013 (top) and 04/02/2014 (bottom). For each night we report the C_N^2 profile as reconstructed with a 62 vertical levels and with 173 levels. These results have been obtained with the standard C_N^2 algorithm (see Report - Phase A). It is possible to observe that, with 173 levels it is possible to put in evidence a few thinner layers, however, the temporal evolution of the C_N^2 (not shown here - see *.pptx

[2]The 99 levels of Meso-Nh give a vertical resolution in the free atmosphere of the order of 300 m up to around 20 km. The 173 levels of Meso-Nh give a vertical resolution in the free atmosphere of the order of 150 m up to around 20 km.

in the BSCW), does not produce and improvement on the temporal variability of the turbulence in the free atmosphere.

If we repeat the experiment using the new algorithm for the C_N^2 (Eq.2) Fig.64 we observe that the C_N^2 profile obtained with 62 levels presents layers much more defined close to the ground as well as in the free atmosphere. If we consider 173 levels the model is able to resolve a larger number of layers much more thinner the previous ones. Looking at the temporal evolution of the C_N^2 profiles (Fig.65) it is possible to observe that, during the night, the evolution of the layers in the free atmosphere presents a high level of variability with layers that are triggered and then disappear at different heights above the ground. If we look at Fig.66 we can see that the higher is vertical resolution (larger number of layers and thinner layers) the larger is the temporal variability of the seeing in the free atmosphere. We highlight that these tests have been done with a non calibrated model. The calibration should be repeated with 173 vertical levels. **However the important message/result here is that we proved that, with the new C_N^2 algorithm, it is possible to reconstruct a turbulence stratification with a vertical resolution that is that required by a few more sophisticated systems of WFAO such as the MCAO and the MOAO. In Masciadri et al., 2013 [50] are reported the typical vertical resolution required for LTAO (Δh $\sim$ 670 m with FOV = 1-2 arcmin), MCAO (Δh $\sim$ 450 m with FOV = 2-3 arcmin) and MOAO (Δh $\sim$ 134 m with FOV = 5-10 arcmin).**

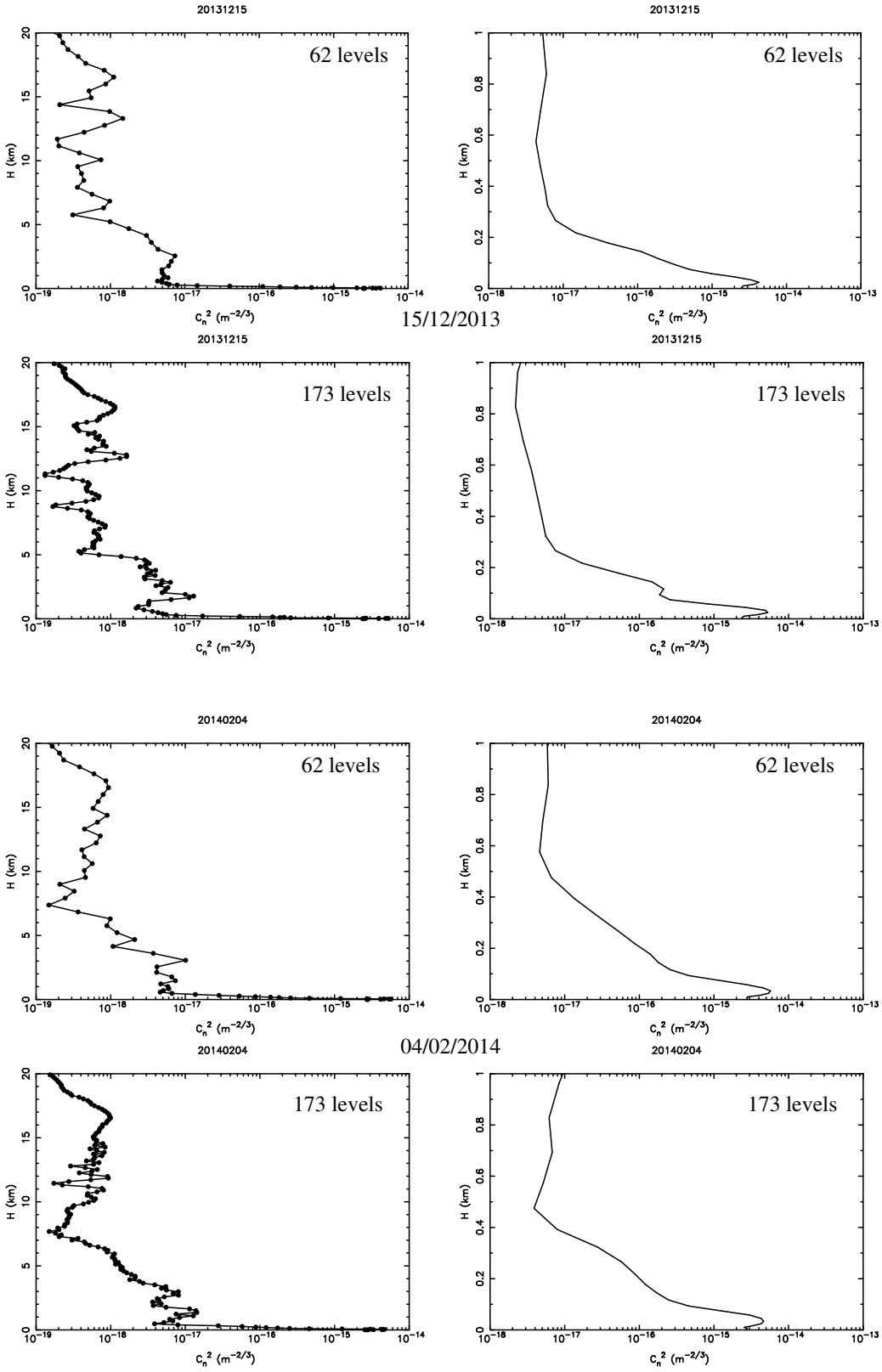

Figure 63: Vertical profiles of the average simulated C_N^2 (standard algorithm) with different vertical resolutions, for a night in 2013 (top 4) and a night in 2014 (bottom 4), at 62 and 173 levels.

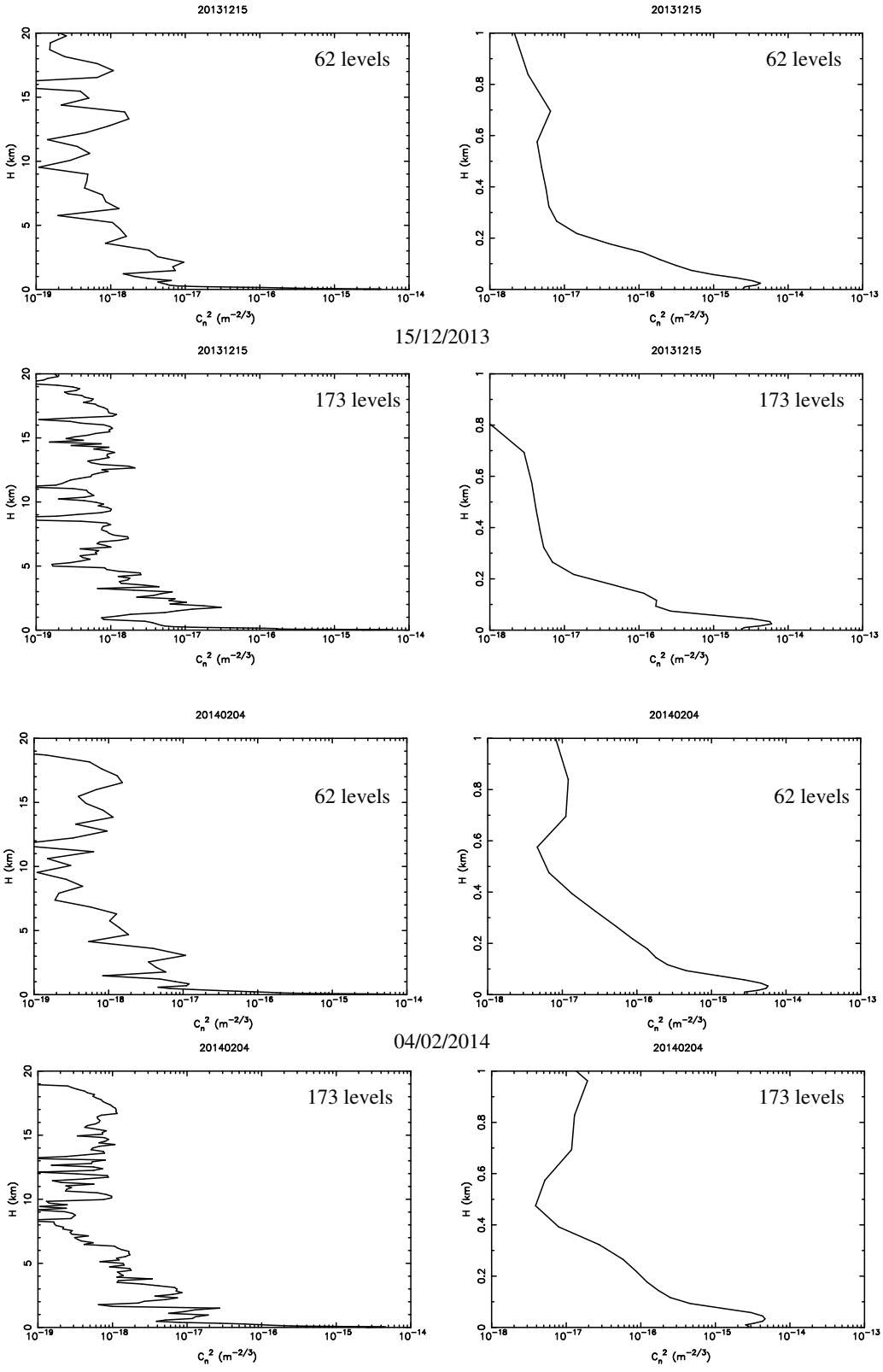

Figure 64: Vertical profiles of the average simulated C_N^2 with different vertical resolutions, for a night in 2013 (top 4) and a night in 2014 (bottom 4), at 62 and 173 levels. The C_N^2 is corrected with the algorithm of Section 5.

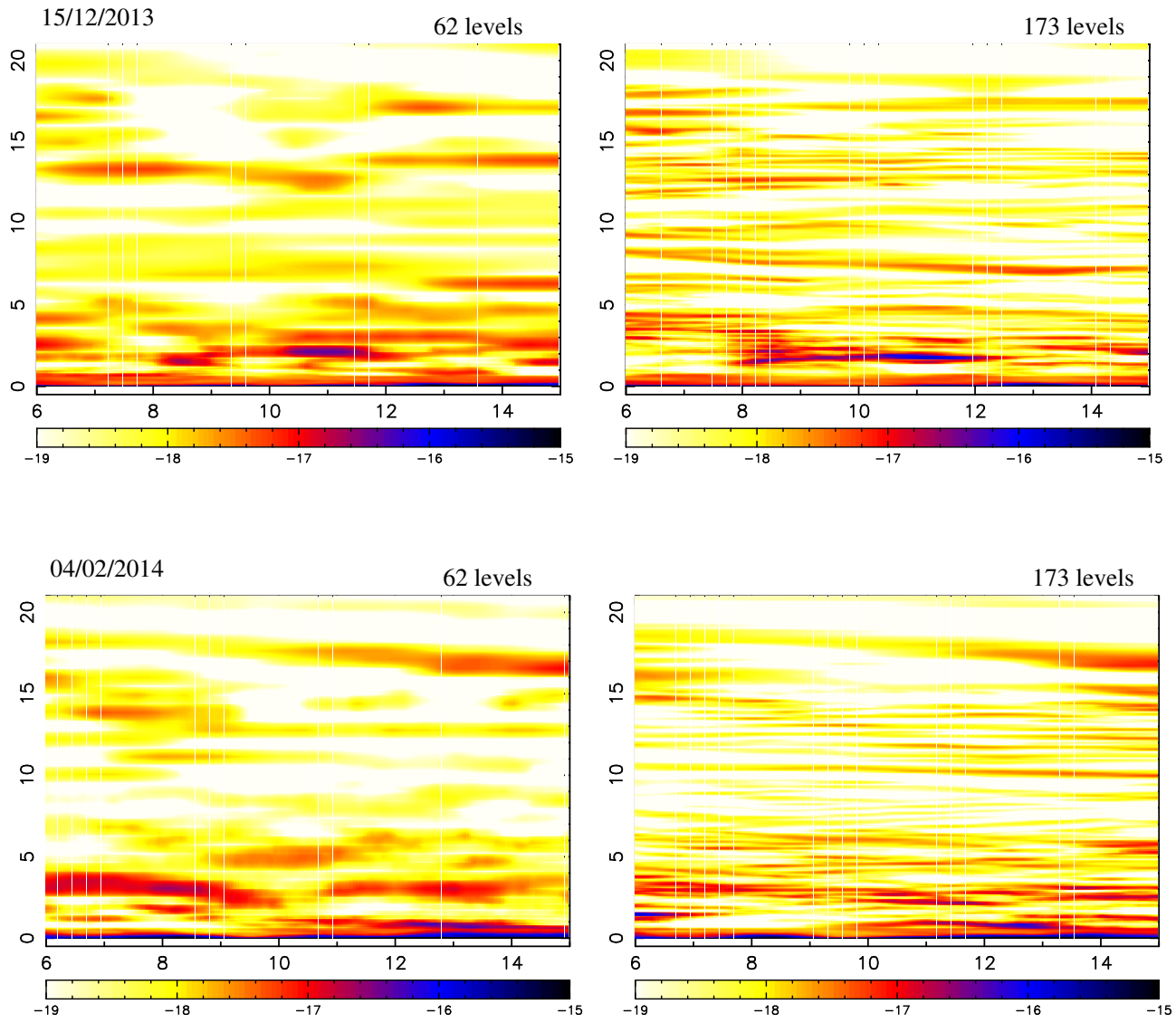

Figure 65: Temporal evolution of the vertical profiles of the simulated C_N^2 with different vertical resolutions, for a night in 2013 (top) and a night in 2014 (bottom), at 62 and 173 levels. The C_N^2 is corrected with the algorithm of Section 5.

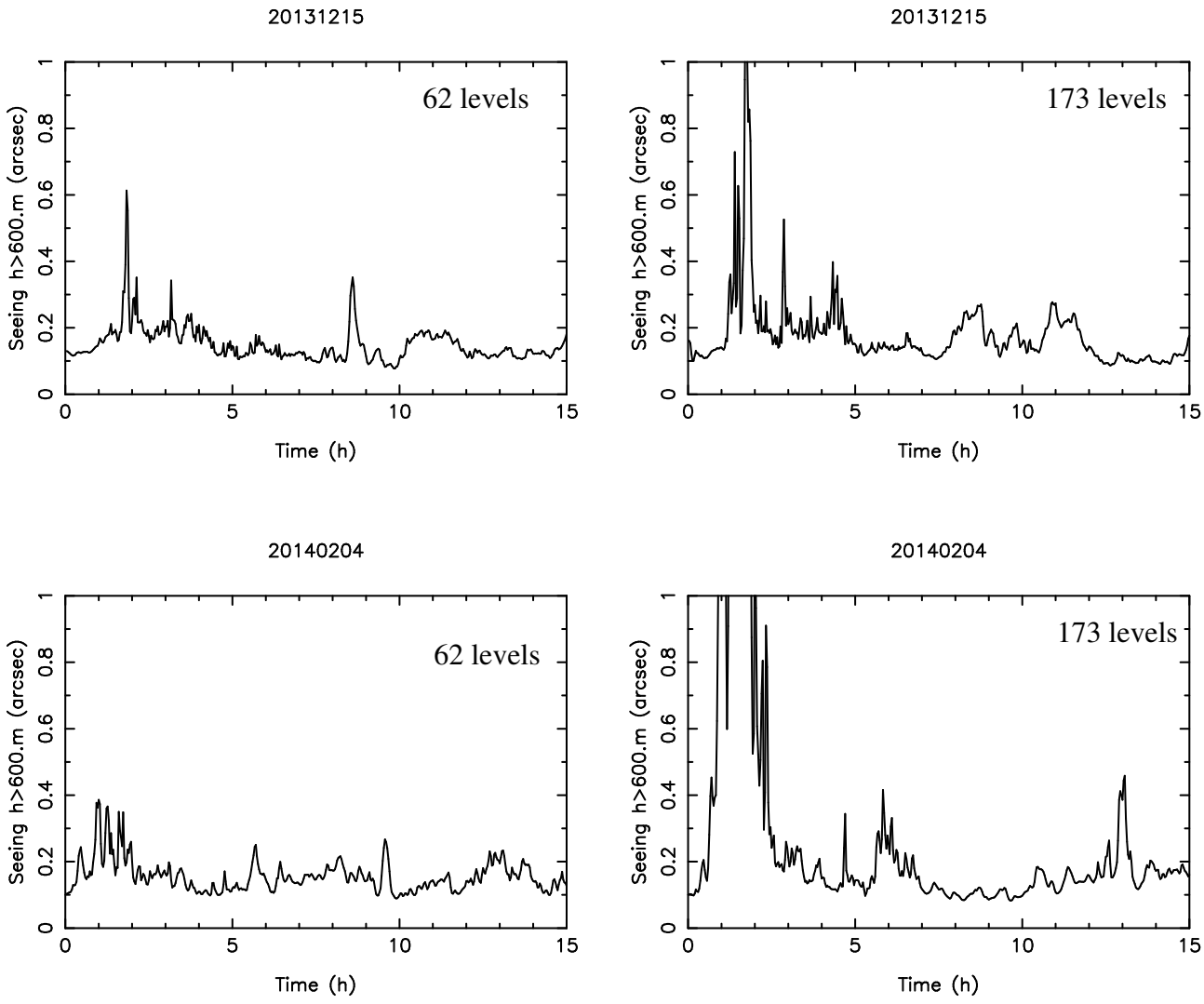

Figure 66: Temporal evolution of the simulated free atmosphere seeing with different vertical resolutions, for a night in 2013 (top) and a night in 2014 (bottom), at 62 and 173 levels. The C_N^2 is corrected with the algorithm of Section 5.

7 Work Package 3.1 - Architecture selection

In this section we present the result of a series of benchmark tests. The goal is to select the most suitable server in order to implement an operational forecast system that can provide useful outputs in less than 17 hours of time (cf. Figure 67).

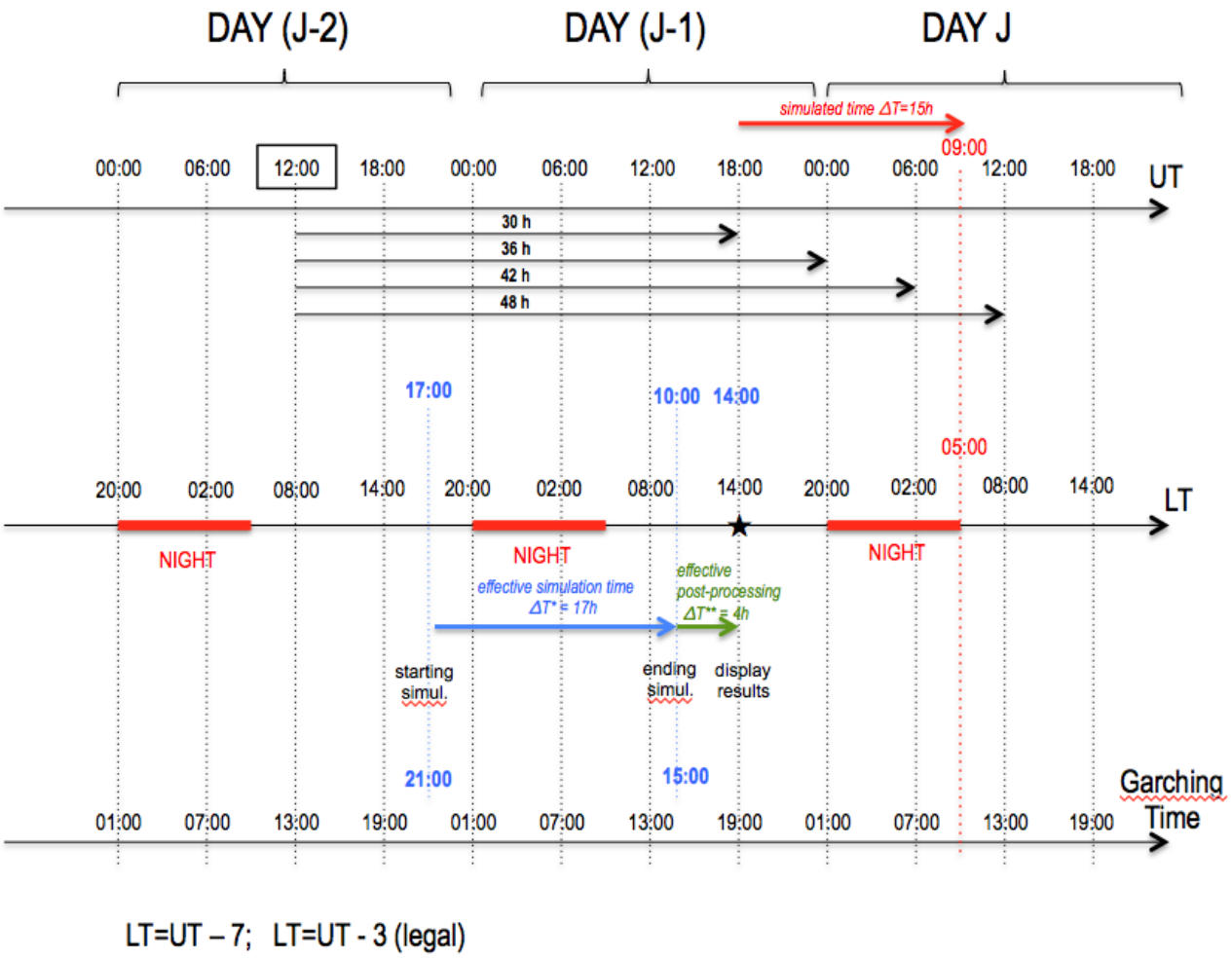

Figure 67: Toy model summarizing all the key informations related to a typical simulation done in a operational context as conceived for the Paranal and Armazones Observatories.

Fig. 67 shows three temporal axes: UT states for universal time; LT for local time at the sites Paranal and Armazones; Garching time indicates the time in the location where the forecast is executed. The black star located on the LT axis indicates the time in which results of the forecasts of the OT and atmospherical parameters related to the night time of the day J have to be displayed[3]. Forecasts products from the ECMWF to be used for the mesoscale model initialization and forcing are calculated by the ECMWF General Circulation Model (CGM) at 00:00 and 12:00 UT. In order to carry out a simulation for the night time of the day J, to post-process and display the results within the temporal constraints we defined, we have to consider forecasts calculated at 12:00 UT of the day (J-2).[4] Table 107 summarizes the sequence of initialization and forcing

[3]We highlight that ESO indicates as optimal limit time (16:00 LT). We decided to maintain 14:00 LT to be more conservative.
[4]This is the most convenient case, i.e. the closest in time with respect to the beginning of the night J. In perspective it will

forecasts for the Meso-Nh model to be used to simulate the atmospheric parameters and the OT of the night time of the day J. We have to start the simulation at 18:00 UT of the day (J-1), simulate 15 hours up to 09:00 UT (05:00 LT) and forcing the model each six hours with the forecasts products coming from the ECMWF GCM (Table 107).

The dealer (Meteo France in our case) of the forecasts products used to initialize the mesoscale model can assure the deliverable of the products within the next 6 successive hours with respect to the time of calculation of the forecast[5]. This means that we can not start the simulation before 14:00 LT of the day (J-2). To be more conservative we consider three more hours and we fix the starting time of the simulation at 17:00 LT of the day (J-2). In the interval included between 17:00 LT of day (J-2) and 14:00 LT of day (J-1) there are 21 hours. We establish the effective time required to perform the simulation equal to $\Delta T^* = 17$ hours and the effective time required to perform the data post-processing equal to $\Delta T^{**} = 4$ hours. These are indicative estimates useful to select the servers suitable for this application. The ratio between ΔT^* and ΔT^{**} can be eventually adjusted in case the necessity appears and the constraints permit that.

7.1 First benchmark

In order to select a commercial server suited for the execution of the atmospheric model in an operational configuration, we have designed a simple benchmark based on standard software (python with scipy/numpy modules). Although the best way to assess the performances of a server with respect of a given application (the Meso-Nh code in our case) is to use the application itself, the effort needed to properly install and run the atmospheric model makes this approach unpractical in many cases or simply heavy. An easier and faster solution is to use a procedure based on standard software usually available on common Linux distributions, or easily installable from default repositories, provided that they give similar results to the application itself. This has to be tested. Because the Meso-Nh model is known to be highly parallelized we designed a very simple benchmark procedure with the purpose of exploiting the parallelization capabilities of the computing server; then we validated the benchmark comparing its results with those of the Meso-NH model (with a short 11-min run) running on the same systems (in their optimized configuration).
The benchmark is based on a computational kernel which computes the 2D cross-correlation on a 2-D array, using the fft algorithm. This is easily implemented with a few lines of python code using the scipy/numpy modules; because of the efficient implementation of the computational algorithm in the modules, the result is not expected to be biased by the interpretive nature of the python language. Obviously what we are interested in is not the computation itself, but the time of execution of the procedure. The computing kernel is executed several time in order to result in a total execution time of a few minutes to rule out the overhead of launching the processes. In order to evaluate the overall parallelization performances a wrapper procedure is used in order to launch a number of identical processes running the computation kernel and gather the execution time data. Using several independent processes to model the performances of a parallelized application is obviously an approximation because usually real world parallel programs are not 100% parallelized.

The benchmark was run on a number of different systems and we selected four of them to show the capability of the benchmark tests to highlight the differences due to different architectures:

- **PETRA** Workstation Fujitsu-Siemens Celsius R670 with 2 Intel Xeon Quad Core, 2.26 GHz, (8 cores), 16 GB RAM;
- **BRAHMA** Server Supermicro with 4 AMD Opteron 16-Core, 2.8 GHz, (64 cores), 128 GB RAM;
- **THORIN** Workstation Intel Core i7-3930K 6-core 3.2 GHz, (6 cores), 64 GB RAM;
- **LTAOMASTER** Server Intel Xeon CPU E7- 4860, 4 CPU 10-Cores, 2.27 Hz (40 cores),128 GB RAM.

be possible to check if it is possible to use for the forcing ECMWF GCM forecasts calculated at 00:00 UT of the day (J-1). It is important to highlight that the time necessary to deliver the data is typically of 6 hours, this means that these new data should be available not before 02:00 LT of the day (J-1).

[5]We highlight that we did not find better solutions at present.

Name	N. CPU	CPU (Processors) Model	Freq. (GHz)	Cores (*)	RAM	R_{multi}	R_{mnh}
PETRA	2	Intel Xeon E25520	2.2	4	16GB	1	1
BRAHMA	4	AMD Opteron 6386SE	2.8	16	128GB	8.3	7.2
THORIN	1	Intel Core i7-3930K	3.2	6	64GB	2.6	1.8
LTAOMASTER	4	Intel Xeon E7- 4860	2.27	10	128GB	3.9	-

* With 'core' we mean 'core for processor'. Core: it is the kernel of a computational unit.
Ex: two cores on one processor is very similar to a bi-processor.

Table 104: Server configurations. In column five, 'Cores' means the number of cores in each CPU. The SI (Eq. 3) ratio between the servers (in their best configurations) are reported in the last two columns (R_{multi}, R_{mnh}), with PETRA as a reference, for the simple procedure in python and for a 11-min Meso-NH run, respectively. R_{multi} is the ratio of the SI index calculated between different server and PETRA taken as a reference with the procedure described in this section run for 11 minutes. R_{mnh} is the ratio of SI calculated for the 11-min run of Meso-Nh (see Section 7.2). R_{mnh} does not appear for LTAOMASTER because after the test done with the procedure described in this section we estimated not necessary to perform tests with the Meso-Nh model.

The configuration of the server is summarized in Table 104. BRAHMA is a relatively high parallel system with a medium CPU speed; PETRA is a moderately parallel system with a lowest speed CPU; THORIN is a system with very fast CPU speed but a lowest level of parallelism than BRAHMA. LTAOMASTER has a low speed CPU. It has a better parallel system than PETRA and THORIN.

PETRA is one of the server on which we performed the MOSE feasibility study. It is a workstation bought on 2006. At the epoch was perfect for research goals. It is not a suitable choice for an operational application. THORIN is a server bought by the colleagues of the AO team for AO simulations (ERIS) on 2013. The cost is lower than BRAHMA (this is the reason why we tested this server). It is suitable for code (such as the AO code) not highly parallelized. BRAHMA is a server conceived for highly parallelized codes. It has 128 GB but we estimated that for our applications 64 GB are enough. LTAOMASTER is the server on which ESO run AO simulation for ELTs.
The results of the performances obtained by the different architectures are reported in Figure 68 (left and middle pictures), where the total time for the execution of a number of concurrent jobs is plotted against the number of concurrent jobs. We highlight that we use the term 'job' as 'process'. The capability of running many concurrent processes is evident for BRAHMA whose total elapsed time increases very slightly until the number of jobs becomes equal or greater than the total number of available cores (64). This is evident in Fig. 68-left and middle pictures. From the same data we have then computed a speed index (SI), proportional to the ratio between the number of concurrent jobs and the total elapsed time (Eq. 3).

$$SI = \frac{100 N_{proc}}{E_T} \tag{3}$$

with N_{proc} the number of concurrent processes and E_T the total elapsed time. As shown in Figure 68 (right) the value of the index plotted against the number of concurrent jobs increases approximately linearly until the available cores (16x4 for BRAHAM for example) are saturated by the processes to execute, as expected. To estimate the gain of an architecture with respect to another one we calculate the ratio of the SI of each server with respect to the slowest server (PETRA) obtained by running the python procedure and the actual atmospheric model for short 11-min run (see Table 104 - R_{multi} and R_{mnh}). The value of R_{multi} calculated between different architectures provides us an order of magnitude of the ratio between the total computational time required on the different architectures. It is already visible that BRAHMA architecture is the most suitable for the kind of application we are interested in. A more precise estimate is obtained running the model on the respective servers for the whole duration of the simulation. Such a computation is described in the next section.

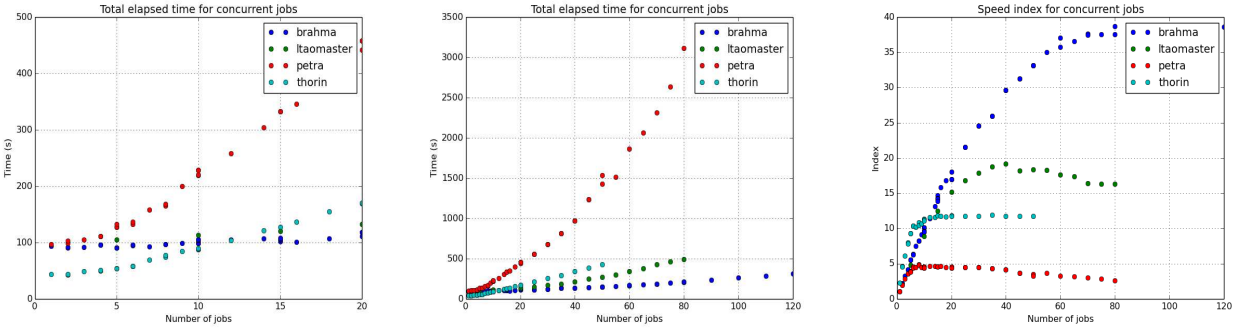

Figure 68: Left and Middle: Total time for the execution of concurrent jobs vs. the number of concurrent jobs for the four systems LTAOMASTER, BRAHMA, PETRA and THORIN. Picture on the left reports a zoom of picture in the middle. Right: SI (Speed Index, see Eq. 3) vs. the number of concurrent jobs. The higher the SI, the faster the system.

7.2 Complete simulation

As we are interested to know wether a computing system is able or not to perform an operational forecast in not more than 17 hours, the only way to answer this critical question is to perform an entire simulation with the Meso-NH model and compare the elapsed times between the beginning and the end of the simulation.
The benchmark consists in a 15-hours run (i.e. the real time we should simulate during an operational simulation) of the night of the 24 December 2007, with the Meso-NH model, and the Astro-Meso-NH package (for the Optical Turbulence) active (ON) (see Fig. 67). Two different configurations have been analyzed: one with three imbricated domains with the finest horizontal resolution of 500 m ("Optical Turbulence" runs), and one with five imbricated domains with the finest horizontal resolution of 100 m ("Atmospherical Parameters" runs). This last solution, taking into account five imbricated domain, considers the case in which just one simulation, simultaneously done above the two sites of Cerro Paranal and Cerro Armazones, is performed. This is the most expensive case in terms on computing resources. ESO might decide also to run in an independent way simulations on the two astronomical sites on two independent servers (option that, obviously, would require minor effective computation time on each individual server) but, considering that this a feasibility study, we decided to test the architecture with the suitable characteristics to respect the most stringent constraints. Two different versions of the model have been used. The M484 version used for the MOSE feasibility study, and a more recent one, the M512 version, having a different numerical scheme allowing for longer time steps and, therefore, shorter computing time. In the new wind advection scheme the 'forward-in-time' (FIT) temporal scheme is used instead of the 'leap-frog' temporal scheme. In the leap-frog method the calculation of the parameter P at the time (t+Δt) depends on P at the time (t-Δt) and P at the time t while in the in-forward temporal scheme it depends only on P at the time t. It is important to notice that the activation of the Astro-Meso-NH package does not imply an increase of the elapsed computed time. The servers tested are listed below:

- **PETRA** Workstation Fujitsu-Siemens Celsius R670 with 2 Intel Xeon Quad Core 2.26 GHz, for a total of 8 processors, 16 GB RAM;
- **BRAHMA** Server Supermicro with 4 AMD Opteron 16-Core 2.8 GHz, for a total of 64 processors, 128 GB RAM; for more informations).

We have selected for every tested server its own optimized configuration (with respect to the numerical set-up of the Meso-NH simulations), in terms of number of processes used for the parallel runs. We used 8 processes for PETRA and 64 processes for BRAHMA. To see how the computing elapsed time scales with the number of processes, the reader can look at Figure 69 for the presumed best system BRAHMA (for this, only 11-min runs were performed, not the total 15-hour simulation).

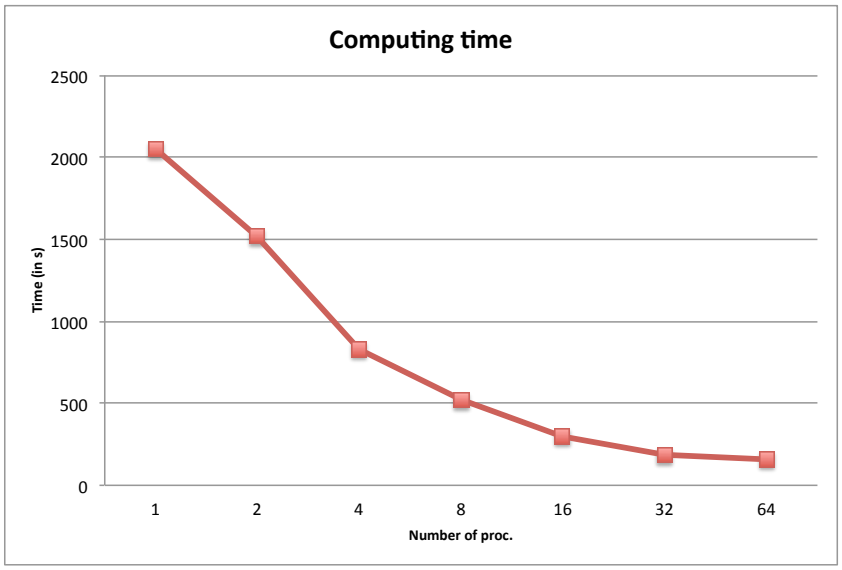

Figure 69: Computing elapsed time vs. number of processes. The server is BRAHMA, and a 11-minutes run with Meso-NH was performed.

Looking at Table 105-top we can see that, with BRAHMA, the specifications required for an operational system ($\Delta T^* = 17$ hours) are easily fulfilled for the $\Delta X = 500$ m configuration (3 DOM) for both versions of the model (M484 and M512), with elapsed time around 2h50min hours (M484) and 1h42min hours (M512). Both cases are well below the identified limit of 17 hours.

Even with the finest $\Delta X = 100$ m resolution (5 DOM), when the simulation is done simultaneously for Paranal and Armazones (worst constraints), the runs remain below this threshold (11h30min) with the M512 version (Table 105-top). We also took into account the fact that, depending on the season, the *night* (i.e. the number of hours of night time) might be more or less long. We therefore considered the more conservative condition of 18 hours of simulations (Table 105-bottom). Also under these conditions, in all cases (3 DOM, 4 DOM and 5 DOM) the simulations duration is below the threshold of 17 hours (maximum elapasd time is 16 hours). **We conclude that the architecture of BRAHMA guarantees to perform the simulations we are interested on even with the maximum horizontal resolution ($\Delta X = 100$ m) running simultaneously on the two sites: Cerro Paranal and Cerro Armazones**. We calculated the phase of post-processing including: extraction of the diagnostic parameters from the binary files, calculation of the content of the figures to be displayed in the web page of the project, compression of data is of around 1 hour therefore we still have **a margin of 4 hours** if we consider the ΔT^* of 17 h plus the ΔT^{**} of 4 h (see Fig.67).

Looking at Table 105 we can see that the ratio between the total computation time between BRAHMA and PETRA is of the order of 10-11 depending on the horizontal resolution used (500 m or 100 m). This is a little bigger than the factor $R_{mnh} = 7.2$ of Table 104 and it means that, considering the whole simulation, the gain of BRAHMA with respect to PETRA is even more effective and **BRAHMA appears 10 times more rapid than PETRA**.
The typical cost for a server as BRAHMA included two hard disk of 2 Tb each is of the order of **11 KEuro**. We estimate that, in an operational configuration, the best comfortable solution should be to have a back-up server to avoid to remain in stand-by in case of break or failure of one server. The second server might also be also used to run a simulation with a 3 DOM for the optical turbulence for Armazones (as we will see in a while).
A few further considerations are indeed important to converge on the final set-up of the system. While for the atmospherical parameters we can use 4 or 5 domains selecting two different sites without any problem, the optical turbulence requires a calibration that in principle can be different from one site to the other. This

15h simulations	3DOM	4DOM	5DOM
PETRA (M484)	31h41min	N/A	N/A
PETRA (M512)	17h01min	N/A	N/A
GAIN	1.86	N/A	N/A
BRAHMA (M484)	2h50min	N/A	19h52min
BRAHMA (M512)	1h42min	7h39min	11h30min
GAIN	1.66	N/A	1.73

18h simulations	3DOM	4DOM	5DOM
PETRA (M484)	38h01min	N/A	N/A
PETRA (M512)	20h25min	N/A	N/A
GAIN	1.86	N/A	N/A
BRAHMA (M484)	3h24min	N/A	23h50min
BRAHMA (M512)	2h02min	9h11min	13h48min
BRAHMA (M512*)	3h03min	10h33min	15h52min
GAIN	1.66	N/A	1.73

Table 105: Results of the benchmark test. 15-hours and 18-hours run of the night of 24 December 2007. Times for a 18-hours run have been extrapolated from the times for a 15-hours run. 3 DOM (ΔX = 500 m); 4 DOM (ΔX = 100 m); 5 DOM (ΔX = 100 m, Paranal and Armazones run simultaneously on the same server). This 18h simulation is useful to take into account the fact that, depending on different seasons, the night can be more or less long. The value of 18h is more conservative. The last line of the table on the bottom (that indicated by an asterisk) considers a surplus of 15% to take into account of the variability of simulations of different nights and of different servers. The calculation has been done only to be extremely conservative.

means that for the optical turbulence is not possible a simultaneous simulation for two different sites. However the optical turbulence is performed with a 3 domain set-up that is characterized by an elapsed time of just 3 hours. We found therefore an 'economical' solution that optimizes the number of runs with the lowest cost. We performed a modification of the code so to be able to do a simulation with 5 domains and retrieve the atmospherical parameters for the two sites. The information of the optical turbulence for one site (Paranal for example) is retrieved from the third domain (the more internal one) of the same simulation. To retrieve the optical turbulence of the second site (Armazones) a model with 3 domains is run just after the first simulation is concluded. Considering the typical time necessary for the simulations (see Table 105-bottom) we should be within the limit imposed by the threshold. In any case, the back-up server might be used too for most of the time (with exception of the emergency cases).

7.3 Data storage

Data storage for one entire simulation of 18 hours is summarized in Table 106 (ΔX=100 m configuration) for the two sites: Paranal and Armazones.

ECMWF FORECAST (LIMITED DOMAIN)	INITIALIZATION and FORCING	SIMULATION OUTPUT (binary files)	SIMULATION OUTPUT (ASCII files)
10 files	55 files	177 files	$\sim$1002 files
0.025 GB	0.5 GB	23 GB	0.5 GB

Total: $\sim$24 GB

Table 106: Number and dimension of the files produced during one entire Meso-Nh simulation (one night) with the 5 domains (ΔX = 100 m) configuration (Note: the size of the global analyses extended on the whole Earth is 9.2 GB).

In the second column are included all the outputs of the $PREP-REAL$ plus SPAWNING, in the third column are included all the binary files of the runs (EXSEG) plus the the outputs of the diacronic files (DIAG). In the fourth column are included all the outputs in ASCII format plus figures to be displayed plus log files. The fourth column includes data that have to be necessarily saved. **If we consider compressed data we calculated, for two astronomical sites, a total of 0.5 Gb for each night and a total of $\sim$ 180 Gb in one year. To store also the binary files on the internal domain (as we suggest) we estimate 1 Tb in one year**.